

THERMAL PERFORMANCE AND SURFACE CHARACTERIZATION OF A SELECTIVE LASER MELTED FLAT-PLATE OSCILLATING HEAT PIPE

J. G. Monroe¹, O. T. Ibrahim¹, S. M. Thompson^{1,2,†}, N. Shamsaei^{1,2}, L. Bian³, A. Elwany⁴

¹ Department of Mechanical Engineering, Mississippi State University, MS 39762 USA

² Center for Advanced Vehicular Systems, Starkville, MS 39759 USA

³ Industrial and Systems Engineering, Mississippi State University, MS 39762 USA

⁴ Industrial and Systems Engineering, Texas A&M University, TX 77843

† Corresponding author:

REVIEWED

Email: thompson@me.msstate.edu

Phone: (662) 325 1535

Abstract

A titanium alloy (Ti-6Al-4V) flat-plate oscillating heat pipe (FP-OHP) was fabricated using Selective Laser Melting (SLM). The 50.8 x 38.1 x 15.75 mm³ FP-OHP consisted of four integral layers of capillary-sized, circular mini-channels (1.52 mm in diameter). The post-SLM prototype was de-powdered using pressurized air and a novel layer-by-layer, plug-and-pressurize design/approach. A vacuum-grade port was threaded into the FP-OHP, and the heat pipe was charged with acetone (~70% by volume) then hermetically sealed. Experiments were conducted to characterize the thermal performance and functionality of the multi-layered FP-OHP. Results indicate that the acetone-filled FP-OHP operates and can provide for an 800% increase in effective thermal conductivity relative to pure Ti-6Al-4V. The build integrity of the FP-OHP was investigated by shearing along its width to inspect the channel-area surface using field emission scanning electron microscopy (SEM) and laser triangulation for channel topography. The mean surface roughness was found to be approximately 45 micrometers and characterized by partially-melted, abraded particles. This study demonstrates the appeal of additive manufacturing for fabrication of customized heat transfer media traditionally challenging to realize.

Introduction

The ongoing miniaturization of electronic components is urgently driving the innovation for efficient, passive and compact cooling systems. In the past, vapor chambers and wicking structures have been used as cooling systems [1–3], but are now demonstrating their limited ability to handle high heat fluxes (e.g. > 100 W/cm²) [4]. The first oscillating heat pipe (OHP), introduced by Akachi circa 1990 [5], is a wickless candidate for efficiently dissipating high heat fluxes in a variety of operating environments (e.g. high gravity, free convection, spot heating, thermal spreading, etc) [6–12]. The oscillating heat pipe, as shown schematically in Fig. 1, is typically constructed from either a serpentine tube ('tubular' OHP) or a flat plate featuring interior channels (FP-OHP). In either case, the capillary-dimension of the channels, coupled with using a suitable working fluid, allows for surface tension to dominate and thus the generation of liquid plugs and vapor bubbles. The OHP is partially filled with a working fluid and, after the internal liquid vaporizes due to sufficient heat transfer, transports thermal energy from the evaporator to condenser via phase-change and forced convection. The serpentine arrangement of

the capillary-scaled channels allows for a highly-transient/non-uniform pressure field to exist in the evaporator. This pressure field works against the plugs in adjacent channels – thus creating oscillatory liquid/vapor displacement and cyclic evaporator replenishment. Gravity magnitude and direction can affect OHP thermal performance [7–10]. Some research has been conducted to reduce the effect of gravity on OHP thermal performance by increasing the number of turns [11], decreasing the channel diameter [12] and using three dimensional (3D) channel layer configurations [11]. Incorporating a 3D design concept into the FP-OHP effectively enhances the channel density by adding multiple layers of channels to improve the heat flux limitation of the OHP. The thermal performance of an OHP mainly depends on the working fluid, filling ratio, its orientation, operating temperature, heating and cooling area, number of serpentine turns, and channel dimensions [6].

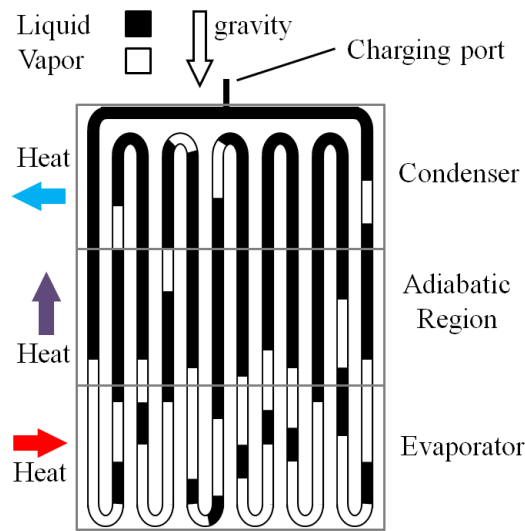


Figure 1. An oscillating heat pipe vertically-aligned with gravity

Since OHP thermal performance, and its effective miniaturization, is highly sensitive to its channel design [12], there have been many research efforts into experimentally characterizing new design concepts and features. There have been OHPs with non-uniform channel cross-section [13], floating ball check valves [14], Tesla-type check valves [15], hybrid tube and flat-plate, silicon material [16] and more. The FP-OHP channel density (*i.e.* channels/volume) is a design feature desirable for high heat flux mitigation and achieving more gravity independence. Over the past several years, research has been conducted on multi-layer FP-OHPs as constructed via traditional, milling/sealing methods. Thompson et al. [17] experimentally investigated a two-layered, ‘3D’ FP-OHP with channels ($1.7 \times 1.175 \text{ mm}^2$) milled along the upper and lower faces of a copper plate. The channels were staggered so that they were not located above or below each other. The FP-OHP was filled with either acetone or water and the heating area, cooling temperature, and operating orientation were varied. The results demonstrated that 3D FP-OHP is less orientation-dependent, especially when the heated area increases for the same input power. The lowest thermal resistance was attained by using water as the working fluid. The heat pipe efficiently managed heat fluxes as high as $\sim 300 \text{ W/cm}^2$ at a total load of 300 W.

Smoot and Ma[18] experimentally investigated a triple-layered, copper FP-OHP. The device consisted of two copper plates with interconnecting channels milled on both sides ($1.6 \times$

1.6 mm² channel cross-section). These two plates, along with two copper cover plates, were brazed together to form three channel layers (two interconnected and one standalone). The performance of the triple-layered OHP was compared with single and double-layered OHPs of similar design. The results demonstrated that the OHP's dissipative capabilities increased by adding more channel layers. The additional layers of channels increased the effective thermal conductivity 361% (comparing the single and triple-layered OHPs) at 5 kW heat input. Finally, the triple-layered OHP was shown to effectively transport 8 kW at a heat flux of 103 W/cm², outperforming both the double- and single-layered FP-OHPs.

Current OHP design parameters - such as channel geometry, number of layers, material selection, etc. - are, and will continue to be, limited by the capabilities of available manufacturing processes. In the past, it has been difficult to incorporate small scale designs or intricate channel networks within a solid object. However, with the introduction and maturation of Selective Laser Melting (SLM), a Powder Bed Fusion-Laser (PBF-L) additive manufacturing (AM) process, complex metallic parts with features unobtainable, or challenging to achieve, via traditional machining/manufacturing processes can now be fabricated [19]. In brief, SLM is a type of laser sintering process that occurs in inert atmosphere for generating dense parts from metallic powder via melt pool formation/solidification by a traveling, focused laser [20]. Melt pool solidification/cooling rates, and thus final microstructural characteristics of SLM parts, are highly-governed by the employed laser scanning techniques[20].

Modern AM processes, such as SLM, have made more complex, multi-layered OHP designs in atypical materials possible. Therefore, in this study, a novel four-layered, titanium alloy (Ti-6Al-4V) FP-OHP is fabricated via SLM and then experimentally characterized to determine its ability to operate and transfer heat. Since the surface condition of a channel structure can impact the heat transfer ability of heat pipes, the SLM/Ti-6Al-4V surface roughness and topology are investigated and discussed.

Prototype Design and Manufacture

As shown in Fig. 2, the four-layered FP-OHP had major dimensions of approximately 5.08 x 3.81 x 1.58 cm³ and consisted of a serpentine-arranged, closed-loop mini-channel with a circular cross-section diameter of 1.52 mm. To ensure that a variety of working fluids would form stable liquid plugs in the capillary channel, the channel diameter was selected as to satisfy Eq. (1):

$$D_{ch} \leq 1.84 \sqrt{\frac{\sigma}{g(\rho_L - \rho_V)}} \quad (1)$$

where σ is the liquid/vapor surface tension, g is the local acceleration due to gravity, ρ_L is the liquid density, and ρ_V is the vapor density.

Using a SLM system (ProX 100™), the FP-OHP was fabricated within a purged argon atmosphere while using manufacture-specified process parameters, *i.e.* laser output power \cong 49 W, scanning speed \cong 400 mm/s, hatch distance \cong 70 μ m and layer thickness \cong 30 μ m. Titanium alloy (Ti-6Al-4V) was chosen as the material since, for many electronics packaging schemes, the coefficient of thermal expansion (CTE) 'mismatch' between the heat source and spreader/sink should be minimized. The mismatch in CTE between Ti-6Al-4V and silicon is

187%; this is an improvement over more common thermal management materials such as copper (453% mismatch) or aluminum (640% mismatch). The Ti-6Al-4V powder (ASTM B347 Grade 5) was spherical in shape with a diameter range of 15-45 μm and a Ti-6Al-4V build plate (10 x 10 x 1 cm^3) was utilized. The total build time for the FP-OHP was 16 hours. After the SLM procedure, the FP-OHP was carefully sheared off the build plate using Electrical Discharge Machining (EDM), and the top and bottom surfaces were end-milled/faced (~ 0.1 mm removed) to obtain a smooth finish.

Due to the nature of the SLM process, the channels within the FP-OHP were packed with unmelted, Ti-6Al-4V powder. This unmelted powder had provided much-needed support for preventing channel collapse during the build. In order to clear the trapped powder from the closed-loop OHP channel, two 'vent' ports along each channel layer, as shown in Fig. 2, were utilized. Powder was removed by pressuring one vent hole per channel layer with water and air (~ 1 MPa), while leaving the corresponding-layer vent hole open to atmospheric pressure. After an individual layer was cleared, the corresponding vent holes were sealed using titanium screws (either 0-80 UNF or 2-56 UNC) so that the next layer could be effectively cleared. Once all powder was removed, the screws were secured in place with vacuum-grade epoxy (Loctite 222 Threadlocker). The circular protrusion (*i.e.* fill port) on the FP-OHP allowed for a copper capillary tube to be connected via a 3.18 mm NPT stainless steel fitting (Swagelok SS-1-UT-1-2). To test the success of the de-powdering process and ensure channel continuity, the FP-OHP was completely filled with acetone; then the inserted liquid volume was compared with the ideal channel volume of the FP-OHP's CAD (Computer Aided Drawing) solid model. After removing the acetone the FP-OHP was charged with ~ 2.4 mL of HPLC grade acetone ($\sim 70\%$ by volume), and the copper capillary tube was pneumatically crimped to form a hermetic seal.

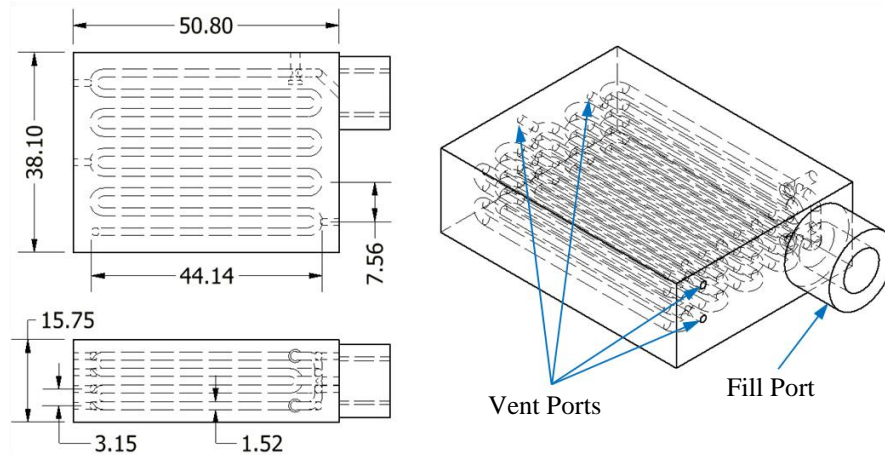


Figure 2. Ti-6Al-4V FP-OHP design with dimensions (dimensions in mm)

Thermal Characterization - Procedure and Setup

The acetone-filled FP-OHP was tested to ensure its hermeticity and to characterize its thermal performance. Hence, as shown in Fig. 3, one portion ($\sim 25 \times 38.1$ mm^2) of the FP-OHP was uniformly heated, with a firmly-attached hot plate, while a portion ($\sim 25 \times 38.1$ mm^2) of its opposite/reverse face was cooled via a firmly-attached water block. Thermal paste (Omega, Omegatherm 201) was applied to the hot plate and water block surfaces in contact with the FP-

OHP to minimize thermal contact resistance. The water block, which consisted of two 8.7 mm circular channels for in-series flow, was continuously supplied with deionized water at 20 °C by a temperature-controlled water circulator/bath (PolyScience AD15R-30-A11B). The hot plate was heated via two, embedded 150 W cartridge heaters (Watlow FIREROD, 6.35 mm OD). Power supplied to the cartridge heaters was controlled by a Variac and measured/confirmed with a digital multimeter (DMM). Sixteen T-type thermocouples (Omega, ± 1 °C) were affixed to the surfaces of the FP-OHP and were connected to a data acquisition system (National Instruments cDAQ-9178 chassis with NI 9213 temperature module) for recording. The DAQ was able to measure temperature differences as low as 0.25 °C. Fiberglass insulation was wrapped around the heated/cooled FP-OHP to minimize heat loss to environment (estimated to be $\lesssim 3\%$ power input) and the device was oriented vertically-along gravity (*i.e.* bottom-heating). A full experimental schematic along with the thermocouple locations can be seen below in Fig. 3.

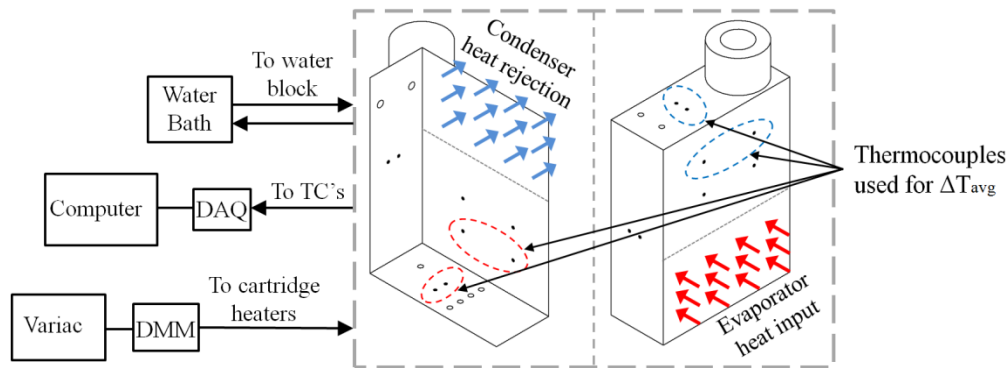


Figure 3. Experimental setup and thermocouple locations

Testing began when the FP-OHP was isothermal with the cooling water (*i.e.* at 20 °C). Power was applied at 5 W increments. Upon introduction of each new heat input, the FP-OHP temperature response was monitored until it was clear that a pseudo-steady-state was achieved; thereupon, the steady-state temperature field was recorded for approximately three minutes. This process was repeated until the OHP power input reached 50 W. In order to provide a baseline for the water acetone FP-OHP thermal performance, the experimental procedure was repeated on an empty (and open to atmosphere) FP-OHP. However, the empty test was terminated once the maximum FP-OHP temperature reached 150 °C at 35 W.

Thermal Characterization

To quantify the thermal performance of the FP-OHP, its effective thermal conductivity, k_{eff} , was estimated using Eq. (2). For this estimation, the heat transfer through the FP-OHP was assumed to be approximately equal to electrical power, P , and unidirectional along a line between the center of the evaporator and condenser ($L = 29.9$ mm).

$$k_{eff} \approx \frac{P}{A_c} \frac{L}{\Delta T_{avg}} \quad (2)$$

The average temperature difference across the FP-OHP, ΔT_{avg} , was taken as difference between the spatiotemporal average of thermocouple measurements in the evaporator and condenser, as shown in Fig. 3. The total cross-sectional area, A_c , of the OHP was taken as 38.1 x

15.75 mm². Using Eq. (2), the effective thermal conductivity of the FP-OHP, when partially-filled with acetone (~70%) and empty, is shown in Fig. 4.

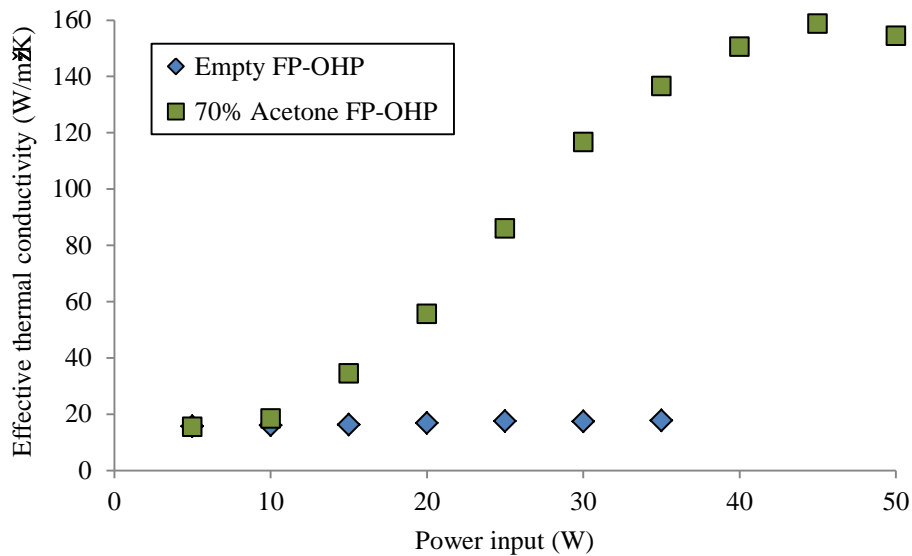


Figure 4. Effective thermal conductivity of the acetone-filled and empty FP-OHP

From Fig. 4, it may be seen that the empty and acetone-filled FP-OHP have similar effective thermal conductivity at low power inputs (e.g. $P \lesssim 10$ W) – when the OHP is not operating (*i.e.* the fluid inside is not oscillating). After the OHP fluid activity was initiated (*i.e.* $P \sim 15$ W), the effective thermal conductivity of the FP-OHP increases non-linearly with power until ~ 45 W when it peaks at ~ 159 W/m²·K. The effective thermal conductivity of the empty FP-OHP remains near-constant at ~ 17 W/m²·K. This is marginally higher than the tabulated thermal conductivity of Ti-6Al-4V (6.7 W/m²·K), and this is due to the defined, effective thermal conductivity in Eq. (2). However, since the maximum effective thermal conductivity (159 W/m²·K) of the FP-OHP is 846% higher than that of the empty FP-OHP, the benefit and functionality of the FP-OHP is clearly demonstrated. Note that the maximum temperature of the acetone-filled FP-OHP at 50 W was approximately 113°C. These experimental results confirm that that the multi-layered FP-OHP is fully-operable and able to hold a continual hermetic seal.

Channel Surface Characterization

To examine the surface quality of the SLM FP-OHP channel structure, an older prototype was sheared via EDM axially along a layer of channels to expose that layer's surface and then sheared across transversely to show each layer's channel profile. Note that the previous prototype had identical channel dimensions (\varnothing 1.52 mm) and similar channel design. However, the original prototype had an insufficient number of vent holes and could not be successfully de-powdered. Thus it was sectioned for surface imaging while an improved design (with additional vents) was built for thermal testing. The prototype slice was well cleaned with acetone before imaging to remove any surface contamination or debris left from the shearing process.

A field emission scanning electron microscope (FESEM) (Zeiss SUPRA 40) was used for detailed imaging of the channel surface, while laser triangulation (Taylor-Hobson Talysurf CLI 2000) was used to quantify channel surface topography. Figure 5 shows the FP-OHP slice used

in channel surface characterization. Imaging was performed on 3 of the 11 exposed channel sections, *i.e.* channels 2, 5, and 9 (or C2, C5, C9).

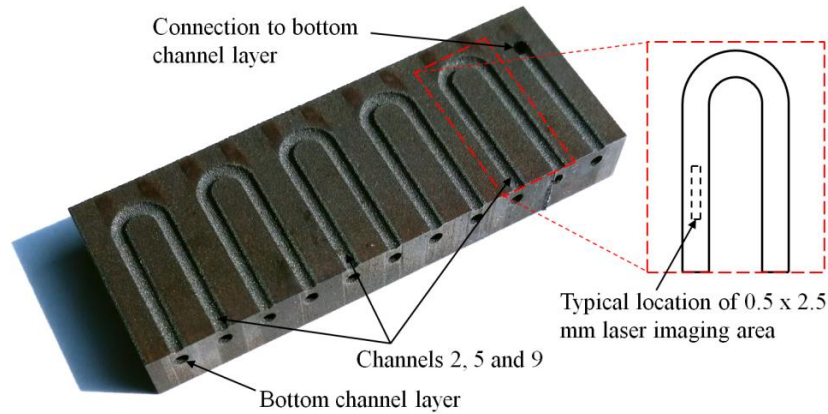


Figure 5. Slice of FP-OHP with imaging locations and channels-of-interest (C2, C5 and C9)

FESEM images of C2 are shown in Fig. 6. In Fig. 6a, the roughness of the raw channel surface is clearly seen, especially compared with that of the EDM surface visible along the top and bottom edges of the image. Figure 6b magnifies a portion of the channel to reveal individual Ti-6Al-4V particles that were on the boundary of the melt zone during manufacturing. Note that the diameter of all measured particles in Fig. 6b falls within the manufacturer-specified powder size (15-45 μm).

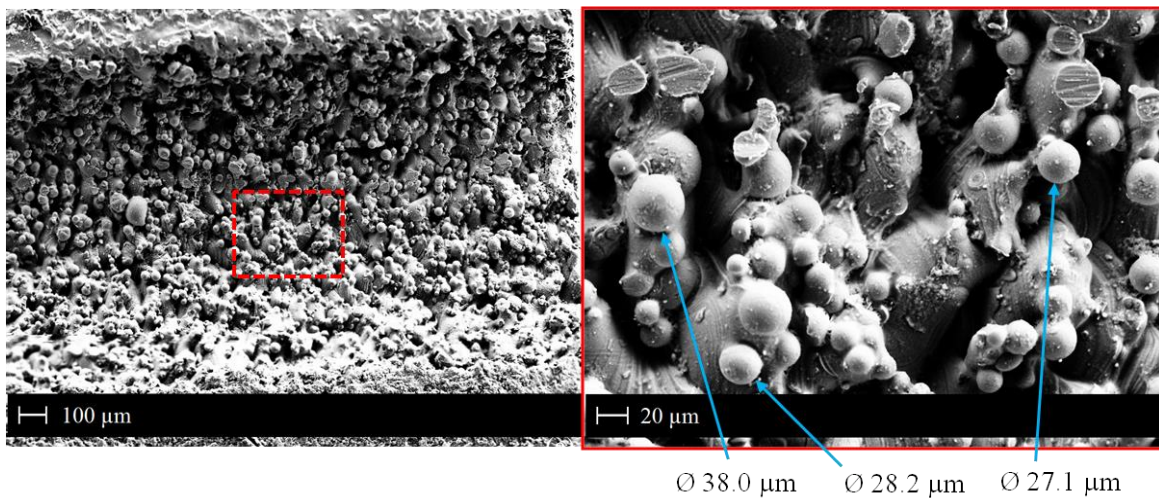


Figure 6. SEM images of C2 at (a) 100 micron and (b) 20 micron magnification

The surface topography, or surface roughness, was measured for each of the three imaging channels within the specified measurement area shown in Fig. 5. A typical trend is shown in Fig. 7, which shows the topography of C5. For a given differential slice along the length of the channel, the surface height in Fig. 7 is seen to vary by $\sim 80 \mu\text{m}$.

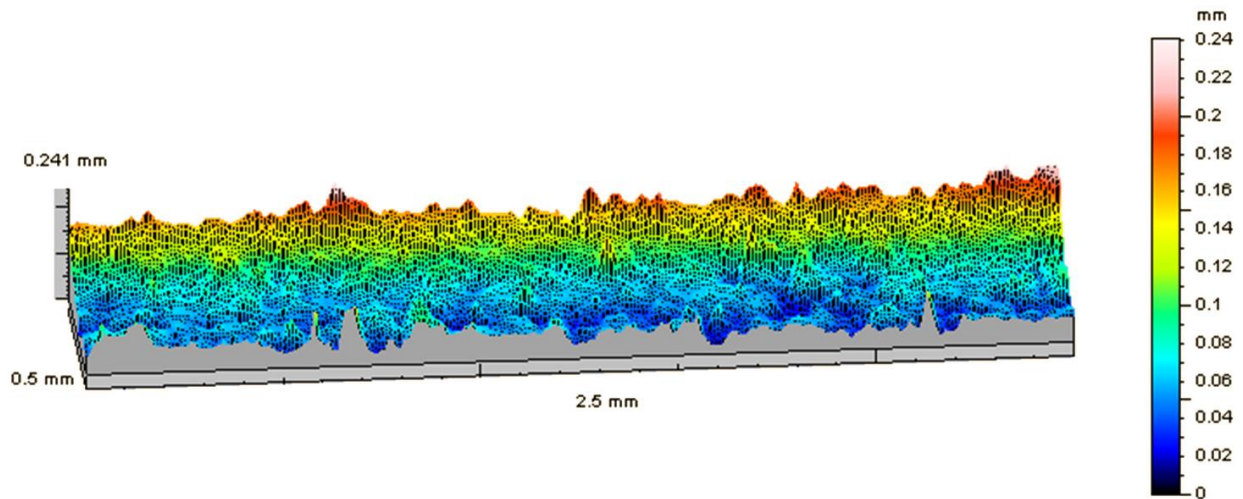


Figure 7. Topography (surface roughness) of a 0.5 x 2.5 mm² section along C5 channel

The curvature of the circular channel wall is very distinct in Fig. 7, despite the narrowness of the imaging area employed. Therefore, the raw surface results obtained from each channel were adjusted (*i.e.* flattened) with a least squares method that removed the general curvature of the surface while retaining local surface roughness. The flattened topography of each channel is given in Fig. 8.

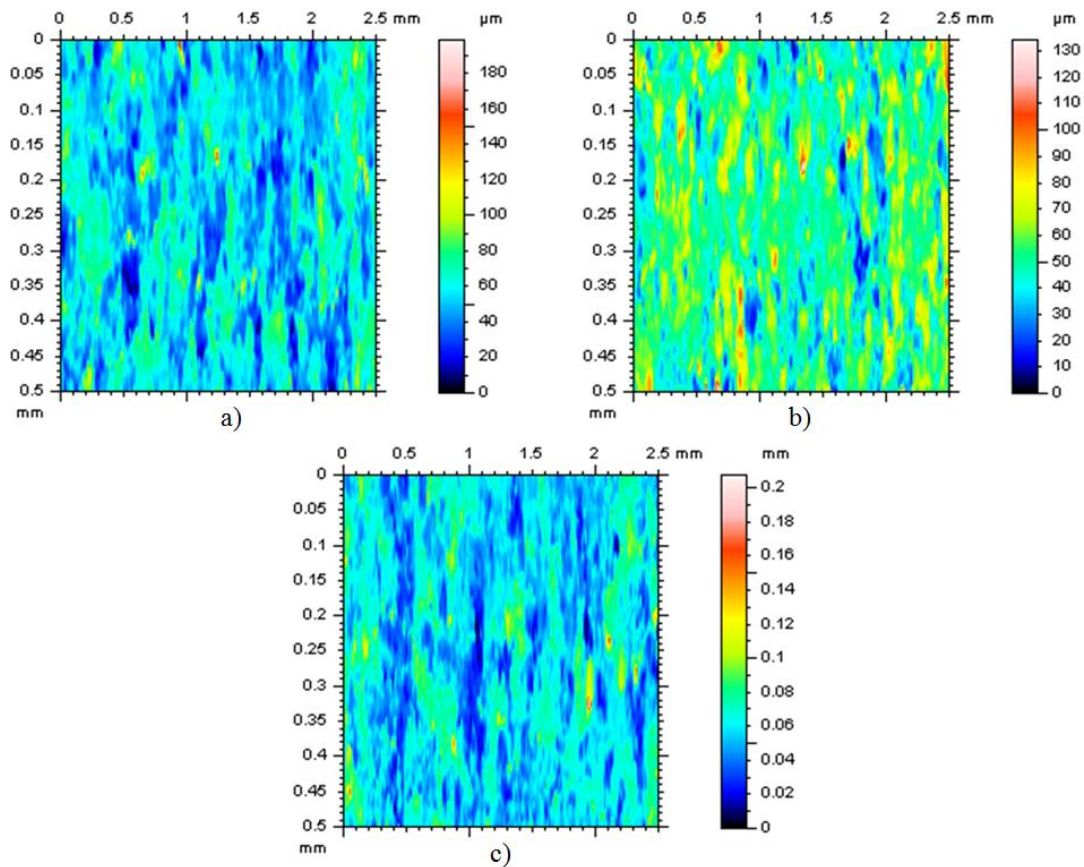


Figure 8. Adjusted (*i.e.* flattened) surface topography for a) C2, b) C5, and c) C9 channels

From Fig. 8 it can be seen that, although there can be local height differences of up to 120-200 μm , most of the surface profile is within a $\sim 85 \mu\text{m}$ band. The height (h) distribution for the three surfaces is given in Table 1.

Table 1. Surface height distribution of adjusted profiles for C2, C5 and C9 channel sections

	$< 25\mu\text{m}$	$25\mu\text{m} < h < 110\mu\text{m}$	$> 110\mu\text{m}$
C2	2.40%	97.4%	0.192%
C5	2.40%	97.5%	0.082%
C9	2.03%	97.6%	0.383%

Note that the roughness of the FP-OHP channel surface, inadvertently induced via the SLM process, will impact the heat transfer of the OHP. Since thin film evaporation is a dominant heat transfer mechanism in the evaporator, the surface-to-wall wetting behavior (e.g. contact angle, meniscus formation) will depend on the surface roughness and condition. The dominant sensible energy transfer between the evaporator and condenser, accomplished via forced convection of the liquid, will be impacted by the surface roughness as the channel frictional head loss is higher.

The benefit/cost of the SLM channels for the OHP may depend on the final OHP operating conditions/application. For instance, the surface roughness can contribute to earlier start-up (*i.e.* activation at lower heat fluxes) of the FP-OHP due to boiling enhancements and secondary capillary action. As shown by Smoot and Ma [21], sintered OHP channels (hybrid vapor chamber OHP) can reduce the start-up power, but can also reduce the power limitation of the OHP – since pressure balancing within the evaporator becomes easier to obtain during operation. Methods such as purging the channels with an acidic solution to etch the sintered particles may be an option for reducing the channel roughness.

Conclusions

Additive manufacturing processes, such as Selective Laser Melting (SLM), are indeed capable of creating functional oscillating heat pipes (OHPs) with previously impossible/unfeasible-to-fabricate geometry. The experimental results demonstrate that a miniature Ti-6Al-4V OHP, with four interconnected channel layers, can maintain a hermetic seal and provide for a 846% percent enhancement in thermal conductivity over pure Ti-6Al-4V with the addition of 2.4 mL of acetone. Surface imaging of a sliced channel layer revealed the Ti-6Al-4V powder particles at the boundary of the melt zone remain predominately distinct and result in local surface height variation $\pm 45 \mu\text{m}$ from the mean. This apparent surface roughness will most likely decrease the start-up power requirement of the OHP. Using AM methods such as SLM, one is now able to incorporate OHPs within the design of any component that requires high heat flux management solutions and to take the technology-readiness of OHPs to the next level.

References

- [1] Chang, J.-Y., Prasher, R. S., Prstic, S., Cheng, P., and Ma, H. B., 2008, “Evaporative Thermal Performance of Vapor Chambers Under Nonuniform Heating Conditions,” *J. Heat Transfer*, **130**(12), p. 121501.

- [2] Lee, S. H.-K., Chu, S. K., Choi, C. C. C., and Jaluria, Y., 2007, "Performance Characteristics of Vapor Chambers with Boiling Enhanced Multi-Wick Structures," Twenty-Third Annual IEEE Semiconductor Thermal Measurement and Management Symposium, IEEE, pp. 125–130.
- [3] Xie, H., Ali, A., and Bhatia, R., 1998, "Use of heat pipes in personal computers," Thermomechanical Phenomena in Electronic Systems -Proceedings of the Intersociety Conference, IEEE, pp. 442–448.
- [4] Peterson, G. P., 1994, An Introduction to Heat Pipes: Modeling, Testing, and Applications, Wiley, New York.
- [5] Akachi, H., 1990, "Structure of a heat pipe," United States Pat.
- [6] Thompson, S. M., Hathaway, A. A., Smoot, C. D., Wilson, C. A., Ma, H. B., Young, R. M., Greenberg, L., Osick, B. R., Campen, S. Van, Morgan, B. C., Sharar, D., and Jankowski, N., 2011, "Robust Thermal Performance of a Flat-Plate Oscillating Heat Pipe During High-Gravity Loading," J. Heat Transfer, **133**(August), p. 104504.
- [7] Khandekar, S., 2003, "Thermofluid Dynamic Study of Flat-Plate Closed-Loop Pulsating Heat Pipes," Microscale Thermophys. Eng., **6**(4), pp. 303–317.
- [8] Borgmeyer, B., and Ma, H., 2007, "Experimental Investigation of Oscillating Motions in a Flat Plate Pulsating Heat Pipe," J. Thermophys. Heat Transf., **21**(2), pp. 405–409.
- [9] Xu, G., Liang, S., and Vogel, M., 2006, "Thermal Characterization of Pulsating Heat Pipes," Thermal and Thermomechanical Proceedings 10th Intersociety Conference on Phenomena in Electronics Systems, 2006. IThERM 2006., IEEE, pp. 552–556.
- [10] Lin, Y. H., Kang, S. W., and Wu, T. Y., 2009, "Fabrication of polydimethylsiloxane (PDMS) pulsating heat pipe," Appl. Therm. Eng., **29**(2-3), pp. 573–580.
- [11] Charoensawan, P., Khandekar, S., Groll, M., and Terdtoon, P., 2003, "Closed loop pulsating heat pipes - Part A: Parametric experimental investigations," Appl. Therm. Eng., **23**(2003), pp. 2009–2020.
- [12] Zhang, Y., and Faghri, A., 2008, "Advances and Unsolved Issues in Pulsating Heat Pipes," Heat Transf. Eng., **29**(1), pp. 20–44.
- [13] Holley, B., and Faghri, A., 2005, "Analysis of pulsating heat pipe with capillary wick and varying channel diameter," Int. J. Heat Mass Transf., **48**, pp. 2635–2651.
- [14] Rittidech, S., Pipatpaiboon, N., and Terdtoon, P., 2007, "Heat-transfer characteristics of a closed-loop oscillating heat-pipe with check valves," Appl. Energy, **84**, pp. 565–577.

- [15] Thompson, S. M., Ma, H. B., and Wilson, C., 2011, "Investigation of a flat-plate oscillating heat pipe with Tesla-type check valves," *Exp. Therm. Fluid Sci.*, **35**, pp. 1265–1273.
- [16] Qu, J., Wu, H., and Cheng, P., 2012, "Start-up, heat transfer and flow characteristics of silicon-based micro pulsating heat pipes," *Int. J. Heat Mass Transf.*, **55**(21-22), pp. 6109–6120.
- [17] Thompson, S. M., Cheng, P., and Ma, H. B., 2011, "An experimental investigation of a three-dimensional flat-plate oscillating heat pipe with staggered microchannels," *Int. J. Heat Mass Transf.*, **54**, pp. 3951–3959.
- [18] Smoot, C. D., and Ma, H. B., 2014, "Experimental Investigation of a Three-Layer Oscillating Heat Pipe," *J. Heat Transfer*, **136**(May), p. 051501.
- [19] Tapia, G., and Elwany, A., 2014, "A Review on Process Monitoring and Control in Metal-Based Additive Manufacturing," *J. Manuf. Sci. Eng.*, **136**(6), p. 60801.
- [20] Gebhardt, A., Schmidt, F.-M., Hötter, J.-S., Sokalla, W., and Sokalla, P., 2010, "Additive Manufacturing by selective laser melting the realizer desktop machine and its application for the dental industry," *Phys. Procedia*, **5**(PART 2), pp. 543–549.
- [21] Smoot, C. D., and Ma, H. B., 2011, "An Experimental Investigation of Hybrid Oscillating Heat Pipe," *Front. Heat Pipes*, **2**(2), pp. 1–6.